# Ab Initio Molecular Dynamics of Heme in Cytochrome c

**Sara Furlan,[†] Giovanni La Penna,*[,‡] Lucia Banci,[§] and Carlo Mealli*[,†]**

*Istituto di Chimica dei Composti Organometallici, Consiglio Nazionale delle Ricerche, Via Madonna del Piano 10, 50019 Sesto Fiorentino, Firenze, Italy, Istituto di Studi Macromolecolari, Consiglio Nazionale delle Ricerche, Via De Marini 6, 16149 Genova, Italy, Centro Risonanze Magnetiche, University of Florence, Via Luigi Sacconi 6, 50019 Sesto Fiorentino, Florence, Italy, and Department of Chemistry, University of Florence, Via della Lastruccia 5, 50019 Sesto Fiorentino, Florence, Italy*

*Received: April 28, 2006; In Final Form: October 4, 2006*

Ab initio molecular dynamics (AIMD) calculations, based on the Car−Parrinello method, have been carried out for three models of heme c that is present in cytochrome c. Both the reduced (Fe(II)) and oxidized (Fe(III)) forms have been analyzed. The simplest models (**1R** and **1O**, respectively) consist of a unsubstituted porphyrin (with no side chains) and two axially coordinated imidazole and ethylmethylthioether ligands. Density functional theory optimizations of these models confirm the basic electronic features and are the starting point for building more complex derivatives. AIMD simulations were performed after reaching the thermal stability at $T = 300$ K. The evolution of the Fe−$L_{ax}$ bond strengths is examined together with the relative rotations of the imidazole and methionine about the axial vector, which appear rather independent from each other. The next models (**2R** and **2O**) contain side chains at the heme to better simulate the actual active site. It is observed that two adjacent propionate groups induce some important effects. The axial Fe−S$\delta$ bond is only weakened in **2R** but is definitely cleaved in the oxidized species **2O**. Also the mobility of the Im ligand seems to be reduced by the formation of a strong hydrogen bond that involves the Im N$\delta$1−H$\delta$1 bond and one carboxylate group. In **2O** the interaction becomes so strong that a proton transfer occurs and the propionic acid is formed. Finally, the models **3** include a free *N*-methyl-acetamide molecule to mimic a portion of the protein backbone. This influences the orientation of carboxylate groups and limits the amount of their hydrogen bonding with the Im ligand. Residual electrostatic interactions are maintained, which are still able to modulate the dissociation of the methionine from the heme.

## Introduction

In biological macromolecules, the chemical properties of the active site are strongly influenced by its interaction with the protein environment, this being particularly relevant for metalloproteins. Among the latter, electron-transfer (ET) proteins are characterized by the electron capture/release capabilities of the metallic core (mono-, bi-, or polynuclear) and the different, yet readily accessible, oxidation states of the constituting atoms.[1−4] A basic requirement is that the overall structural changes remain as small as possible to minimize the reorganization energy and maximize the efficiency and rate of the electron-transfer process.[5,6] Therefore, the structural and dynamic properties of the various redox states have been the subject of many experimental[7,8] and theoretical[9] studies aimed to understand, at the atomic level, the effect of the different electronic population on the protein matrix and its environment.

Cytochrome c (cyt c) is a case study among ET proteins for the capability of controlling and modulating reduction potential and ET kinetics,[10−14] for the relations between redox activity and protein folding,[15−19] and for the role of cyt c in cellular apoptosis.[20]

In the mitochondrial monoheme cytochromes c, the c-type heme prosthetic group centered on the Fe ion is connected to the protein matrix through the covalent bonds between the cysteine residues and two vinyl groups of two adjacent pyrrols. The metal is axially coordinated by the N$\epsilon$2 atom of His 18 and by the S$\delta$ atom of the Met80. (The labeling scheme is that used for the yeast mitochondrial cyt c.[21]) The protein exists in reduced (**R**) and oxidized (**O**) states, which contain Fe(II) and Fe(III), respectively.

There is a strict relation between the forces associated with some chemical groups close to the metal and the structural rearrangements that are triggered by changes in the electron density (e.g., cyt c oxidation). The modulation of both the reduction potential and the plasticity of the coordination sphere depend on different factors such as (i) heme's polarity, (ii) exposure of the heme to solvent and counterions, (iii) constraints on the axial metal ligands imposed by the protein structure, (iv) electrostatic interactions between the atoms of the heme or between the protein and the heme and/or coligands. In particular, a significant effect may be due to the interactions between the negative propionate substituents and some positive centers, such as the residues close to the Met80 (namely, Lys79 and Ile81)[10,22] or the iron atom itself. Some screening is also operated by other protein residues that are in close contact with the heme and its ligands (e.g., Pro30). Seventeen out of twenty crystal and solution structures of the cyt c,[23] which appear in the Protein Data Bank,[24] display the N$\delta$1−H$\delta$1 bond of the His18 side chain along the direction of the Fe−$C_{meso}$ vector in between two propionate heme side chains. Moreover, the structures (with one exception) also show a hydrogen bond that involves the

* Authors to whom correspondence should be addressed. E-mail: lapenna@ge.ismac.cnr.it; carlo.mealli@iccom.cnr.it.
[†] Istituto di Chimica dei Composti Organometallici.
[‡] Istituto di Studi Macromolecolari.
[§] University of Florence.

10.1021/jp062609d CCC: $37.00 
Published on Web 01/18/2007

mentioned Hδ1 atom and the backbone O of Pro30. In conclusion, the protein architecture constrains the orientation of the heme ligands, thus controlling the properties of the active site.

To clarify the peculiar role of the heme propionate side chains in cyt c, we have carried out molecular dynamics (MD) simulations on some cyt c models of the active site by using the Car−Parrinello (CP) method.[25] This performs ab initio molecular dynamics (AIMD) simulations in the time order of picoseconds, thus allowing us to probe structural transitions as a function of the temperature. These aspects are a peculiarity of the CP method. The latter is successfully applied in many fields of chemistry and biology,[26,27] and it is particularly useful to analyze reactions in metalloproteins, associated, for instance, with the variation of metal oxidation and/or spin states. In these cases, the usage of the more manageable semiempirical force fields is hardly applicable.[29]

Quantum mechanics/molecular mechanics (QM/MM) methods have been successfully applied to study the reaction mechanisms in highly detailed models of cytochromes.[30,31] Conversely, only the simplest model of cytochrome c has been investigated up to now with the CP method.[32] Our present approach compares systems of increasing complexity. In fact, rather than considering the entire protein, our modeling explicitly introduces the chemical groups that may affect the redox potential and the mobility of the active site in a stepwise manner. In particular, the attention is focused on the heme's propionate groups and a portion of the protein backbone (Pro30), which strongly interacts with His18 and screens the effects of the propionate groups. In summary, our approach starts with a completely unsubstituted heme model, to which two adjacent side chains with terminal proprionate groups are later added. Finally, the third model includes a free *N*-methyl-acetamide molecule to partially mimic a portion of the protein backbone. With this strategy, the electrostatic interactions between the propionate groups and the axial ligands can be highlighted as well as the role of the hydrogen bonding that is established between the imidazole ligand and the free molecule. The implications for the general properties of cyt c are discussed.

## Methods

**DFT and AIMD Simulations.** The models adopted are schematized in Chart 1, namely, **1**(**R**,**O**), **2**(**R**,**O**), and **3**(**R**,**O**). The first one corresponds to the species already studied by other authors[32,33] and features imidazole (Im) and ethylmethylthioether (EMT) as axial ligands with no substituents at the porphyrin ring. Model **2** includes two propionate and other side chains (e.g., $-CH(CH_3)S(CH_3)$) at the porphyrin. For convenience, the axial methionine is modeled by the simpler dimethyl sulfide (DMS) molecule, while the Im ligand carries an additional methyl substituent. Finally, model **3** contains an additional noncovalently bound *N*-methyl-acetamide (NMA) molecule which, similarly to the protein's Pro30 backbone, can interact with His18 via the hydrogen bond between the NMA carbonyl O and the Hδ1 of Im. During the MD simulations, NMA was kept fixed in space because in cyt c Pro30 belongs to one protein's turn, i.e., a protein portion particularly constrained in its conformation and location. Noteworthy, the $-CH(CH_3)S(CH_3)$ groups used in model **2** are replaced by two simple ethyl substituents in model **3** to limit the overall complexity of the system and speed up the calculations.

The geometries of the models **1R** and **1O** were first optimized with classic density functional theory (DFT) calculations by using the ADF program[34] and the PW91[35] exchange−correlation (XC) potential. The basis sets were DZP for H and S, DZP-1s frozen core for C, TZP-1s frozen core for N, and TZP-2p frozen core for Fe. Spin-restricted and unrestricted calculations were performed, respectively, for Fe(II) and Fe(III) derivatives ($S$ = 0 and $^1/_2$, respectively). No other spin state was explored also in view of the relative experimental information available for pseudo-octahedral iron systems where a heme is axially coordinated by two coligands.[36,37] The coordinates optimized for **1R** and **1O** were used also to start the corresponding CP simulations. Conversely, for the more complex models **2R**, **2O**, **3R**, and **3O** the initial coordinates were those derived from the available NMR structural analyses. These data are present in the Protein Data Bank (PDB codes 1YFC[21] (reduced form, structure 1 in PDB file) and 1YIC[22] (oxidized form, structure 1)). The position of NMA, which has been included to mimic Pro30, is determined based on that of Pro30 as found in the published NMR structures.

The CP method was applied to evaluate the MD trajectories under the conditions of a classical adiabatic energy scale separation between the nuclear and the electronic degrees of freedom. The usage of the extended Lagrangian eliminates the need for solving the self-consistent electronic structure problem at each time step (as required by the Born−Oppenheimer MD approach), but the interaction potentials are calculated on the fly. A parallel version of the Quantum-ESPRESSO package[38] was used with Vanderbilt ultrasoft pseudopotentials[39,40] and the PBE[41] XC functional. The wave functions were expanded in plane waves up to an energy cutoff of 25 Ry, while a 250 Ry cutoff was used for the necessary expansion of the augmented charge density in the proximity of heavy atoms. Periodic boundary conditions (PBCs) were imposed by placing the molecule in an orthorhombic cell and ensuring a minimum separation of 8 Å between periodic replica.

**CHART 1: General Structure of All the Studied Cyt c Models**[a]

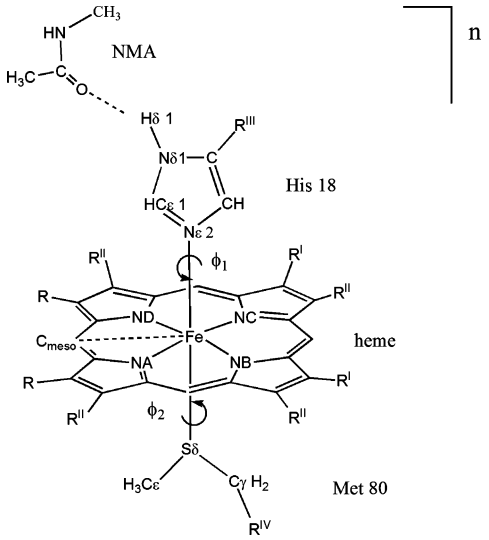


[a] For **1**, R = $R^I$ = $R^{II}$ = $R^{III}$ = H; $R^{IV}$ = $CH_3$−; $n$ = 0, +1. For **2**, R = $(CO_2)(CH_2)_2$−; $R^I$ = $(CH_3)(SCH_3)CH$−; $R^{II}$ = $R^{III}$ = $CH_3$−; $R^{IV}$ = H; $n$ = −2, −1. For **3**, R = $(CO_2)(CH_2)_2$−; $R^I$ = $CH_3CH_2$−; $R^{II}$ = $R^{III}$ = $CH_3$−; $R^{IV}$ = H; $n$ = −2, −1. For **4**, R = $(CO_2)(CH_2)_2$−; $R^I$ = $CH_3CH_2$−; $R^{II}$ = $CH_3$−; $R^{III}$ = $R^{IV}$ = $CH_3CH_2$−; $n$ = −2, −1. The NMA molecule is present in model **3** only. The structure defines the dihedral angles $\phi_1$ and $\phi_2$ for the orientation of the imidazole and thioether ligands. $\phi_1$ is 0° when the Fe−$C_{meso}$ vector lies in the Im plane, and $\phi_2$ is 0° when the Sδ−Cϵ vector projects over the Fe−$C_{meso}$ one.

**TABLE 1: Selected Distances (Å) and Dihedral Angles (deg) for the ADF-Optimized Models 1R and 1O and Other Comparable Data Available from the Literature**

| | **1R**[a] | **1O**[a] | **1R**[b] | **1O**[b] | **1R**[c] | **1O**[c] | **1R**[e] | **1O**[e] | **R**[f] | **O**[g] |
|---|---|---|---|---|---|---|---|---|---|---|
| $d_1$ Fe−N$\epsilon$2(Im) | 1.99 | 1.99 | 1.99 | 1.97 | 2.04 | 2.04 | 2.05 | 2.02 | 1.99 | 1.85 |
| $d_2$ Fe−S$\delta$(EMT) | 2.34 | 2.37 | 2.44 | 2.47 | 2.23 | 2.27 | | | 2.55 | 2.19 |
| $d_3$ Fe−N(heme) | 1.99 | 1.99 | 2.01 | 2.00 | 2.00 | 2.01 | 2.02 | 2.03 | 1.99 | 2.01 |
| $\phi_1$ | 0 | 0 | −1[d] | 1[d] | −54[d] | −59[d] | | | −7 | 9 |
| $\phi_2$ | 165 | 166 | −146[d] | −145[d] | 41[d] | 38[d] | | | 21 | 180 |

[a] This work. [b] Equivalent of model **1** optimized with the standard DFT method in ref 33. [c] Equivalent of model **1** optimized with the CP method in ref 30. [d] For consistency with our results, the $\phi_1$ and $\phi_2$ magnitudes (differently defined in refs 33 and 30) are normalized by adding the values of −45° and −135°, respectively. [e] The bis-imidazole−heme model optimized with the standard DFT method as described in ref 44. [f] Experimental results from ref 21. [g] Experimental results from ref 22.

In **1R**, **2R**, and **3R**, the numbers of atoms and electrons are 58/172, 106/300, and 110/306, respectively. All the MD calculations have been carried out under spin-restricted conditions ($S = 0$ for **R** models and $S = {}^1/_2$ for **O** models). The simulations were performed through sequences of five stages by operating as follows:

1. Electronic energy minimization with fixed atomic positions.

2. Energy minimization with respect to atomic and electronic degrees of freedom to attain the equilibrium geometries.

3. Molecular dynamics simulation of 0.25 ps at constant total energy (i.e., without controlling temperature).

4. Two subsequent molecular dynamics simulations of 0.25 ps at the temperatures of 100 and 200 K, respectively, with the single Nosé−Hoover thermostat[42] coupled to the ionic degrees of freedom.

5. A longer molecular dynamics simulation of 3 ps at a temperature of 300 K by using the same thermostat as in the previous two simulations.

Stages 3 and 4 (thermalization) are necessary to approach slowly the room temperature and to avoid that temperature oscillations affect the electronic features of the ground state. The velocity Verlet algorithm[43] for integrating the equation of motion was used with a time step of 0.12 fs. The calculations were performed on a Linux cluster of computers using 5−10 processors, depending on the size of the molecular models.

**Structural Parameters.** In all cases, the conformational landscape has been explored in detail at $T = 300$ K. In the analysis of the computational results, the following key structural parameters are considered for all models (refer to Chart 1 for atom labeling and definitions): (i) $\phi_1$ is the dihedral angle C$\epsilon$1(Im)−N$\epsilon$2(Im)−Fe(heme)−$C_{meso}$(heme), which describes the orientation of the imidazole axial ligand with respect to the heme plane. By definition, $\phi_1$ is 0° when the Fe−$C_{meso}$ vector lies in the plane of the Im ligand. (ii) $\phi_2$ is the dihedral angle C$\epsilon$(DMS)−S$\delta$(DMS)−Fe(heme)−$C_{meso}$(heme), which describes the orientation of the methionine axial ligand with respect to the heme's plane. When $\phi_2$ is 0°, the S$\delta$−C$\epsilon$ vector projects over the Fe−$C_{meso}$ one. (iii) The $d_1$ and $d_2$ distances refer to the vectors N$\epsilon$2(Im)−Fe and S$\delta$−Fe, respectively.

## Results

**Analysis of the Optimized Geometry.** The analysis of the simplest cyt c model **1**, which features an unsubstituted iron−porphyrin unit and the trans-axial Im and EMT iron ligands, allows understanding some basic features of the cyt c active site. Although the model was already studied by others,[32,33] a standard DFT optimization with the ADF package[34] was carried out to verify the basic electronic aspects of the redox couple **1R** and **1O** and also to attain a suitable geometry for the subsequent MD study. Table 1 compares the important geometrical parameters $d_1$, $d_2$, $\phi_1$, and $\phi_2$ (defined in Chart 1) also with respect to the available experimental[21,22] and computational[32,33] data.

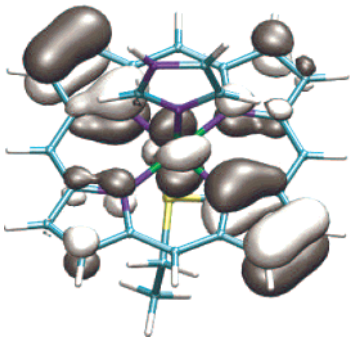

**Figure 1.** Singly occupied molecular orbital of model **1O**.

The Fe−S$\delta$ bond is lengthened by approximately 0.03 Å upon one-electron oxidation of the system. A similar difference had been observed previously,[32,33] although this parameter is affected by some uncertainty. In fact, our optimized values of 2.34 and 2.37 Å for **1R** and **1O**, respectively, differ as much ±0.1 Å with respect to the previous calculations. This is attributable not only to the usage of different algorithms and basis sets but also to a flat potential energy surface (PES) describing the metal coordination, which is fully consistent with the small Fe−S$\delta$ binding energy of 4 kcal $mol^{-1}$, which has been previously reported.[32]

Some useful considerations may be drawn from the analysis of the frontier molecular orbitals (MOs) and in particular of the level that is depopulated upon oxidation. In fact, the singly occupied molecular orbital (SOMO) of **1O** has a prevailing metal $d_{xz}$ character (a $t_{2g}$ level in the pseudo-octahedral geometry of the complex) with sizable antibonding contributions from a $\pi$ level of the heme, as shown in Figure 1. An analysis of the spin density in the SOMO assigns 97% metal character to the unpaired electron. Such a quantitative result confirms that the oxidation largely corresponds to the Fe(II) → Fe(III) transformation and is not ligand-based. At variance with **1R**, the filled $d_{yz}$ orbital of **1O** is no more degenerate with the singly populated $d_{xz}$ one, but somewhat more stable. Predictably, the different electron populations of the two levels affect the rotation of the two axial ligands about the Fe−N and Fe−S bonds, respectively. It has been previously pointed out[45] that the rotations of the trans-axial ligands are important for the function of cytochromes and that the ligands may affect the rotational freedom of each other. Singly faced $\pi$ orbitals of the Im and of methionine do not find equivalent metal $d_\pi$ orbitals upon 90° rotations. Such a MO picture can have some important implication for model **2O**, in which the Fe−S$\delta$ bond is definitely broken (vide infra).

Also, a bis-imidazole−heme model has been previously studied at the DFT and Hartree−Fock levels.[46] Indirect evidence that the second Im ligand may be relatively a stronger donor than the methionine is provided by the sizably weaker trans

**TABLE 2: Average Fe−Nϵ2 ($d_1$), Fe−Sδ ($d_2$), and Fe−N(heme) ($d_3$) Distances (Å) in All of the Studied Models[a]**

| model | 1R | 1O | 2R | 2O | 3R | 3O |
|---|---|---|---|---|---|---|
| $d_1$ | 2.02 (0.05) | 2.03 (0.08) | 2.06 (0.10) | 1.94 (0.07) | 2.00 (0.10) | 1.94 (0.09) |
| $d_2$ | 2.37 (0.10) | 2.42 (0.17) | 2.35 (0.12) | > 3 | 2.60 (0.37) | > 3 |
| $d_3$ | 2.00 (0.05) | 2.00 (0.06) | 2.00 (0.06) | 1.99 (0.07) | 2.00 (0.07) | 1.99 (0.06) |

[a] Root-mean-square errors are within parentheses.

influence that the methionine exerts on the Fe−Nϵ2 bond. In fact, as shown in Table 1, one Fe−Nϵ2 bond is clearly more elongated by the nitrogen than by the sulfur trans-donor (2.05 vs 1.99 Å and 2.02 vs 1.99 Å, for the **R** and **O** forms, respectively).

**Molecular Dynamics.** After general considerations of the static geometries of models **1R** and **1O**, the MD trajectories at 300 K for the systematically more complex models **1**, **2**, and **3** are compared. Consider that the introduction of the propionate substituents at two contiguous pyrrole rings add two negative charges in the system so that the models **2R**/**3R** and **2O**/**3O** become dianionic and monoanionic, respectively. Model **3**, with some minor changes such as the removal of the Cys side chains, has been tailored to study the effect generated by the addition to model **2** of the external and discrete molecule $CH_3(CO)$-$NHCH_3$. The latter, by simulating an amino acid of the protein backbone, should prevent direct contacts between the axial Im ligand and the carboxylate groups of the propionate substituents. Noteworthy, the models **3R** and **3O** do not contain the cysteine substituents at the heme that are present in the **2R** and **2O** analogues. The deletion of Cys side chains helps to speed up the AIMD simulations of the more complex system while it does not affect significantly the chemical model.

The metal−ligand distances, averaged over the trajectories at 300 K, are reported in Table 2 together with the root-mean-square (rms) errors.

The Fe−Sδ separation is always longer than the Fe−Nϵ2 one. On average, the $d_1$ parameter remains almost constant in going from **1R** to **1O**, while the $d_2$ parameter is longer by approximately 0.05 Å in **1O** than in **1R**. From the rms errors and from the analysis of the time evolution of these parameters (data not shown), it is evident that both $d_1$ and $d_2$ span a larger range in the oxidized form than in the reduced one, this aspect being particularly evident for $d_2$. This confirms an intrinsically weaker Fe−Sδ bond, as observed from similar calculations where the thermal effects were not yet introduced.[32]

At 300 K, as a significant effect of the propionate groups in models **2** and **3**, there is an early cleavage of the Fe−S bond. In fact, the $d_2$ distance becomes larger than 3 Å after 0.1 and 0.2 ps for **2O** and **3O**, respectively. However, the role of the temperature is also very important in this respect. In fact, the cleavage does not take place for any model at 200 K, thus showing that the presence of the propionates as porphyrin substituents determines a thermally accessible Fe−S dissociation. As another aspect, the iron−imidazole interaction is evidently affected by the trans methionine ligand. In fact, upon the Fe−Sδ dissociation in **2O** and **3O**, the average $d_1$ parameter becomes significantly shorter than that in **1O** (see average values in Table 2). Mutual influence between the trans-axial ligands has been pointed out for similar heme systems.[30]

The $d_1$ and $d_2$ average values (Table 2) suggest that the Fe−S linkage is generally much weaker than the Fe−N one. The Fe−Sδ cleavage, which occurs in the early stage of the **3O** trajectory, is featured (over a limited period of time) also by **3R** and is likely the cause of the large rms value for $d_2$ found in this case. The analysis of the time evolution of $d_1$ and $d_2$ in **3R** (data not shown) shows that the Fe−Sδ bond is broken only for a fraction

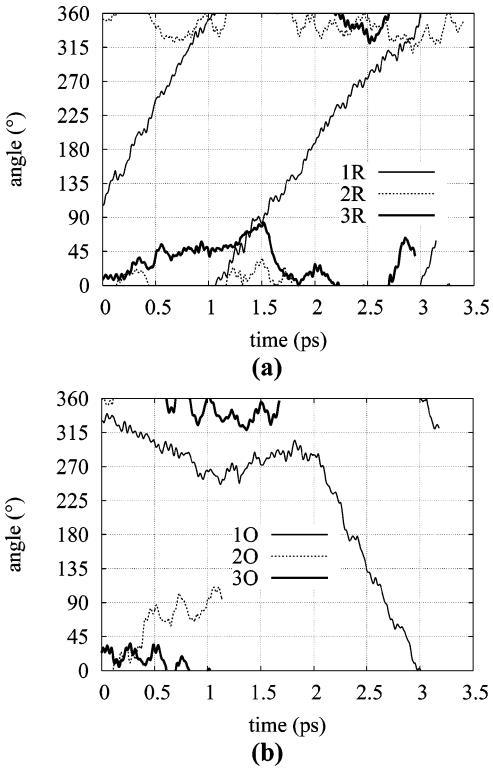


**Figure 2.** Trajectory of the $\phi_1$ dihedral angle for all of the models. (a) Reduced state: **1R** (solid thin line), **2R** (dotted line), and **3R** (solid thick line). (b) Oxidized state: **1O** (solid thin line), **2O** (dotted line), and **3O** (solid thick line). The conformation observed at $t = 0$ is that of the previously thermalized system up to $T = 300$ K. For models **2O** and **3O** the analysis is limited to 1−1.5 ps because of the Fe−S bond cleavage.

of time (0.5−1.3 ps) and that there is a correlation between $d_2$ and $d_1$ distances, i.e., when $d_2$ increases $d_1$ becomes decreases. This effect is discussed in more detail below.

The mutual orientation of the trans-axial ligands is analyzed by monitoring the dihedral angles $\phi_1$ and $\phi_2$ (Chart 1).

The time window of 3.2 ps encompasses enough sampling of the whole range for the dihedral angles. In **1R** (Figures 2a and 3a, solid thin lines), similar slopes for $\phi_1$ and $\phi_2$ indicate that the two axial ligands rotate almost at the same rate for the entire period of time; namely, the two ligands rotate freely and independently.

Figures 4a−4d report a succession of structural situations for **1R**, the entire animation being provided as Supporting Information. It appears that the Im plane constantly bisects the C−S−C angle for approximately 2 ps. The succession of structures highlights that also the porphyrin ligand has a degree of flexibility. Nonetheless, the occasionally enhanced puckering toward either axial ligand does not seem to hinder the rotations about the Fe−Nϵ2 and Fe−Sδ bonds. However, the fast rotation of the Im and EMT ligands does not allot sufficient time to the equilibration of the heme's structure for any given spatial arrangement of the axial ligands. In other words, the structural rearrangements of the equatorial and axial ligands seem to be rather independent of each other.

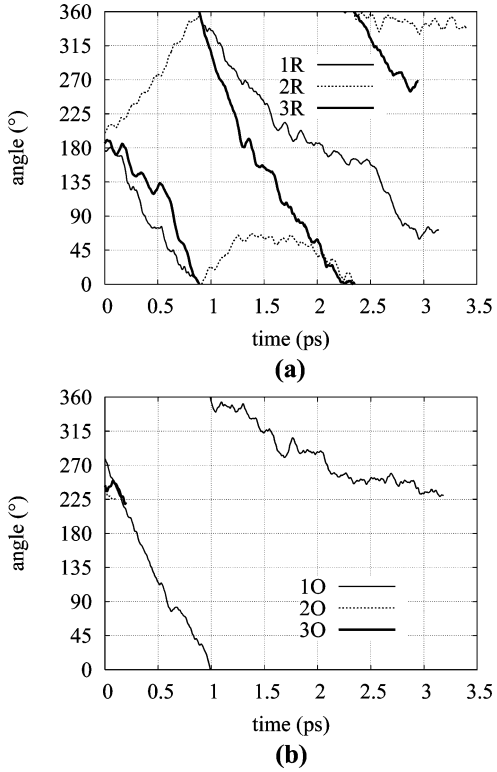


**Figure 3.** Same as for Figure 2 but for the $\phi_2$ dihedral angle. The $\phi_2$ curves are displayed only for the lifetime of the Fe−S$\delta$ bond.

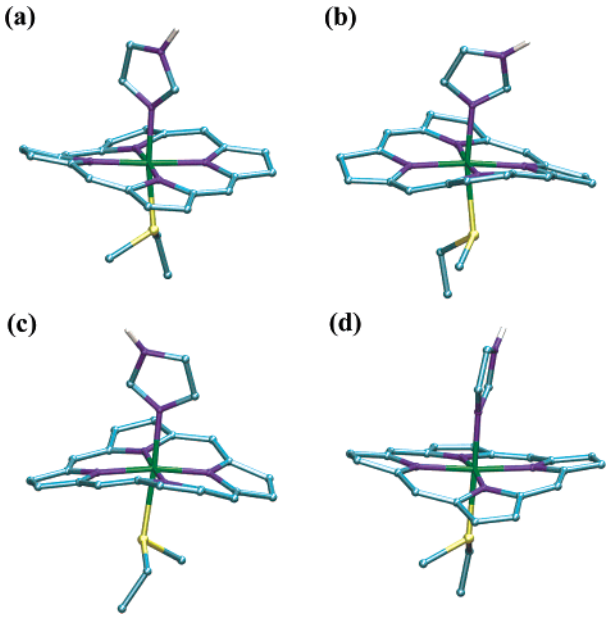


**Figure 4.** Four representative conformations of model **1R** at (a) 0.278, (b) 0.484, (c) 1.161, (d) 2.648 ps of the trajectory. Only H$\delta$1 is displayed among the H atoms.

Remarkably, the $\phi_1$ and $\phi_2$ trajectories follow a somewhat different pattern in **1O** (Figures 2b and 3b, thin lines). In fact, in the first picosecond the mobility of the Im ligand ($\phi_1$) is much reduced with respect to that of the EMT ligand ($\phi_2$). During the second picosecond, the rotation of the Im ligand seems hindered, but also the EMT ligand mobility is significantly reduced. Only in the third picosecond, the Im ligand acquires a relevant rotational freedom while that of the EMT ligand remains limited. The latter aspects are shown in Figure 5, which displays some snapshots along the trajectory of **1O**. The Im orientation is almost unchanged during the first picosecond (parts a−c), while the EMT significantly reorients. The trends are inverted in the third picosecond. Also notice that the porphyrin ring remains much more flattened in **1O** than in **1R** during the whole trajectory (see also animation of **1O** in the Supporting Information).

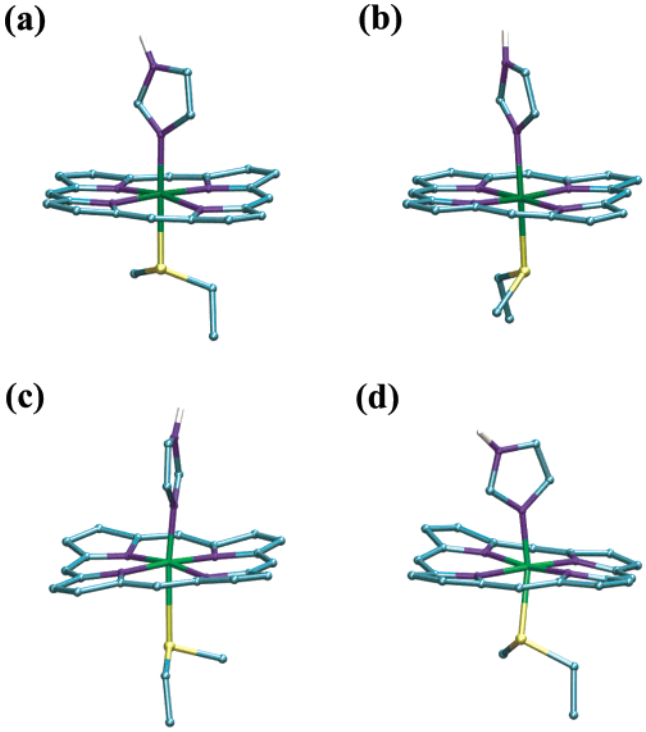


**Figure 5.** Conformations of model **1O** at (a) 0.121, (b) 0.484, (c) 1.330, (d) 2.903 ps of the trajectory. Only H$\delta$1 is displayed among the H atoms.

On average, **1O** exhibits a reduced mobility of the Im ligand with respect to **1R**. As mentioned, the different population of the $d_{xz}$ and $d_{yz}$ orbitals in **1O** (hence the extent of their $\pi$ interactions with the $\pi$ systems of the Im and EMT ligands) may be the electronic property at the origin of the hindered rotation. In any case, the energy barriers for the rotation must be small, since the rotational process at $T = 300$ K is not completely quenched at any time.

Due to the early loss of the methionine ligand, the trend of $\phi_2$ becomes meaningless for models **2O** and **3O**, and the analysis of the $\phi_2$ dihedral angle is interrupted after the first picosecond. In general, the rotational freedom of the Im ligand (Figures 2 and 3, dotted lines) in both **2R** and **2O** derivatives is reduced with respect to that of corresponding models **1**. In **2R**, the $\phi_1$ angle oscillates in the range between −45° and 45° (Figure 2a, dotted line). Conversely, $\phi_2$ (Figure 3a, dotted line) appears to have a larger degree of freedom and seems independent of the value assumed by $\phi_1$. In **2O**, a 90° rotation of the Im ligand is shown during the period of observation, and it is related to the chemical effect illustrated below.

In both the redox forms of models **2** and **3**, hydrogen bonding is possible between one carboxylate oxygen atom of a propionate group and the Im H$\delta$1 atom. The snapshots in Figures 6 and 7 (models **2R** and **2O**) highlight the capability of the propionate groups to form progressively stronger electrostatic interactions with the coordinated Im.

The hydrogen bond is maintained for a longer fraction of time in **2O**, up to the point that the H$\delta$1 proton is transferred from the Im ligand to the carboxylate group with the formation of the propionic acid. As shown in Figure 7c, this occurs after 1 ps, i.e., after the complete cleavage of the iron−sulfur bond.

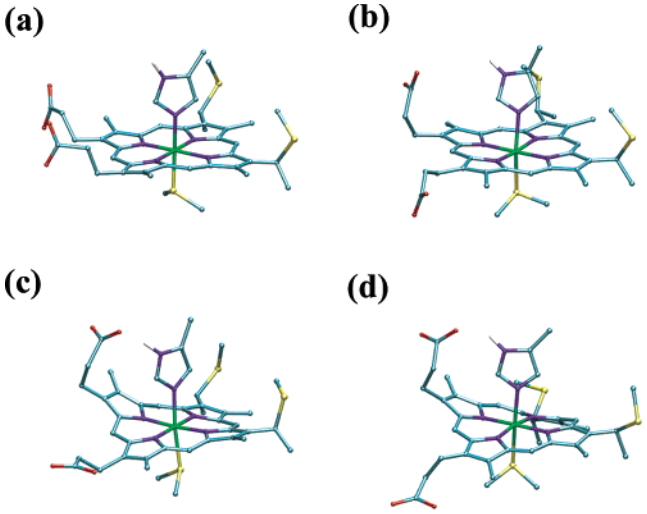


**Figure 6.** Four representative conformations of model **2R** at (a) 0.0, (b) 0.726, (c) 1.209, (d) 3.217 ps of the trajectory. Only H$\delta$1 is displayed among the H atoms.

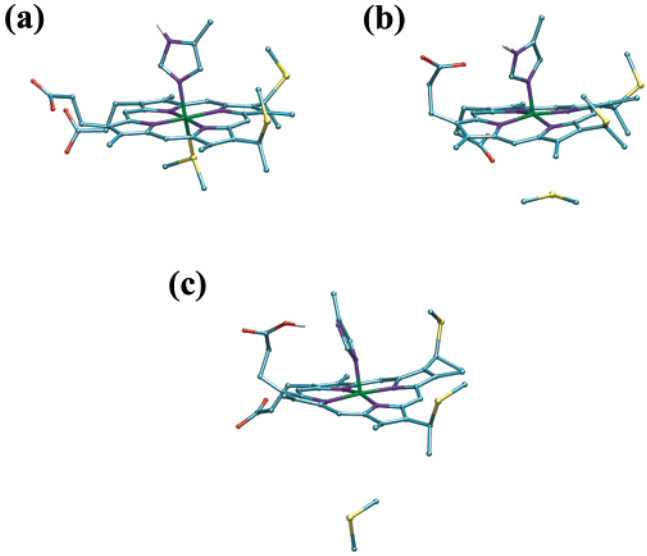


**Figure 7.** Three representative conformations of model **2O** at (a) 0.0, (b) 0.435, (c) 1.137 ps of the trajectory. No further snapshots have been characterized because of the very early Fe−S bond cleavage. Only H$\delta$1 is displayed among the H atoms.

This feature probably can be ascribed to the different basicity exerted by the Im ligand in different metal oxidation states. In fact, the electron deficiency of the metal can be compensated for by an increased donation from Im. Hence, the proton can be more easily abstracted from the N$\delta$1 atom and transferred to the carboxylate. The process also can be kinetically favored by the larger mobility of the Im ligand in **2O** compared to that in **2R** (Figures 2 and 3).

Model **2** shows a strong and direct interaction between one propionate side chain and the Im ligand. However, it should not be forgotten that in the real protein such an interaction may be hindered by other groups within the protein matrix, which prevent the Im and carboxylate groups from being close enough to each other.

In model **2**, the introduction of the propionates and other substituents determines the complete Fe−S bond cleavage in the oxidized form at 300 K. Beside its electronic properties (already outlined for model **1**), the bond is also sensitive to the influence of the electrostatic field created by the propionate groups with their negative charges.

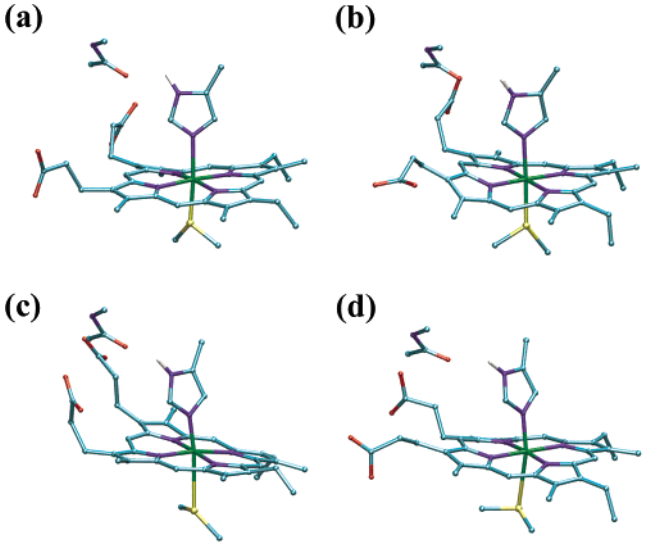


**Figure 8.** Four representative conformations of model **3R** at (a) 0.181, (b) 0.363, (c) 0.726, (d) 1.209 ps of the trajectory. Only H$\delta$1 is displayed among the H atoms.

In **3R**, the rotation of the methionine ligand around the Fe−S$\delta$ bond ($\phi_2$) (Figure 3a, thick solid line) is substantially free, similarly to that observed for the simplest **1R** model. However, the $\phi_1$ rotation (Figure 2a, thick solid line) of the Im ligand appears constrained as in the case of **2R**. In fact, the simulation at 300 K shows an oscillation about the zero angle that corresponds to the configuration in which the Fe−$C_{meso}$ vector and the Im ligand plane are coplanar. On average, the rotational freedom in **3R** and **3O** is similar to that in **2R** and **2O**, and the Im group is not deprotonated in any case. Moreover, there is no indication that the proximity of a peptide-like group in **3** significantly alters the trends. Recall, however, that in **3R** the Fe−S$\delta$ bond is weakened at least for a significant part of the trajectory (0.5−1.3 ps), while, at the same time, the Fe−N$\epsilon$2-(Im) linkage is stable or much less fluctuating. This behavior seems to confirm the previous observations on the easy Fe−S$\delta$ bond breaking in models **2O** and **3O**.

Beside the propionates, also the external amidic C═O group has some capability of forming a hydrogen bond with the H$\delta$1 atom of the Im ligand, as confirmed by the snapshots in Figures 8 and 9. This feature can affect somewhat the basicity of the Im ligand with some consequence for the strength of both axial bonds.

Also, it is noteworthy that in **3R**, while the Fe−S$\delta$ bond is >3 Å, the Im plane and the Fe−$C_{meso}$ vector are no longer coplanar. From Figure 8 and animation 3 provided in the Supporting Information, it may be seen that the major structural changes involve the reorientation of the carboxylate groups of the propionates. A similar rearrangement of one propionate group also occurs for **3O** (Figure 9c), but the Im plane is more strongly constrained in the meso direction (Figure 2b, thick solid line) and the $\phi_1$ rotation is more hindered.

The above observations suggest that the Fe−S$\delta$ bond strength is modulated by the interaction between the Im ligand and the carboxylate group of one propionate side chain. Although this cannot be defined as a clear-cut hydrogen bond, it seems to have a residual electrostatic character that may control the orientation of the Im plane. Recall that the larger the freedom of the Im ligand to rotate away from the Fe−$C_{meso}$ line, the easier the cleavage of the Fe−S$\delta$ bond.

To better estimate the electrostatic interactions involving the propionate groups (independently by the blocking and screening

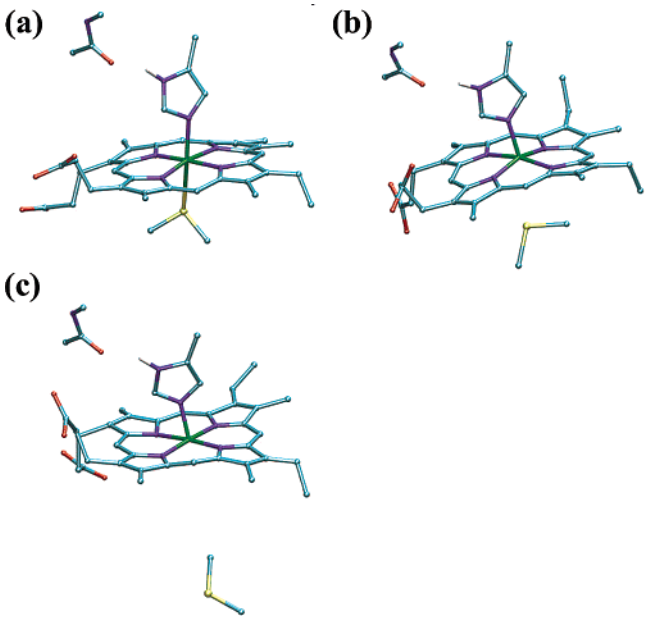


**Figure 9.** Three representative conformations of model **3O** at (a) 0.181, (b) 0.363, (c) 0.726 ps of the trajectory. Only Hδ1 is displayed among the H atoms.

effect of the Pro30 unit), the dynamics of **2O** (i.e., the model without the NMA molecule) were simulated for 1.5 ps at 300 K by fixing in space the propionate side chains. Moreover, the Cα and C$\beta$ portions of the His18 and Met80 ligands were introduced as methyl and methylene groups, respectively (elongation of the groups $R^{III}$ and $R^{IV}$ in Chart 1). The Cα portion was kept fixed. Such an artifact was devised to mimic somehow the constraints imposed by the rigidity of the protein backbone. Again, in this model (**4O**, hereafter) the Fe−Sδ distance elongates over 3 Å as soon as the temperature reaches 300 K. The rotation of the His side chain (plot for the $\phi_1$ angle not shown) is evidently hindered with respect to model **1O**, but it is more free than that in **2O**, where one of the two propionate groups forms a clear-cut hydrogen bond with Hδ1. The Nδ1−Hδ1 bond of the Im ligand is oriented in between the two propionate groups (animation 5 in Supporting Information). The significantly restricted orientation of the Im ligand in models **2O** and **3O** (Figure 2) is a consequence of the hydrogen bond that involves the Hδ1 atom. However, also weaker electrostatic interactions still influence the orientation especially when the distances of the Hδ1 atom from the carboxylate groups become shorter than those observed in the NMR structures. In other words, the extent of the electrostatic interactions depends critically on the positions of the carboxylate groups.

It is noteworthy that even if the Cα positions of the His and Met ligands are fixed a significant rearrangement of the both the His and the Met side chains is possible (animation 5 in Supporting Information). Namely, the flexibility seems sufficient to permit conformational changes even in the presence of a rigid protein backbone.

The nature of the interaction of the substrate with the Im Nδ1−Hδ1 linkage affects the strength of the Fe−Nϵ2 bond, which in turn exerts a variable trans influence over the Fe−Sδ bond and possibly its dissociation. While the latter is not observed in model **1O**, it occurs in all of the oxidized models containing propionate side chains (**2O**, **3O**, and **4O**), either when the propionate groups are close to the Im ligand (**2O**) or when they are forced far from the Im ligand (**4O**). The same event occurs when the Im group forms a hydrogen bond with the protein backbone (**3O**) or with the propionate group itself (**2O**). However, model **4O** shows that Fe−S bond cleavage also occurs when the hydrogen bond is absent.

The easier cleavage of the Fe−Sδ bond in the oxidized form, compared to that in the reduced form, already has been addressed from theoretical studies.[32] Here, for the first time, the effect of propionate groups is highlighted from the molecular dynamics at 300 K. The same effect was proposed by Moore[47] on the basis of experiments, but it has not been theoretically or computationally described yet.

## Conclusions

The AIMD simulations, performed on models of the heme site in cytochrome c with increasing degree of complexity, have highlighted some of the effects which may govern the behavior and the function of cyt c in both the reduced and the oxidized forms. The simplest models **1R** and **1O** with no substituent on the heme have been useful to tune up the MD simulations and to establish a direct reference for the studies of more complex systems. As expected, in model **1** the axial ligands remain both essentially coordinated to the metal center, irrespective of the metal oxidation state. The iron−methionine bond is weaker than the iron−Im one, but there is no major change upon oxidation (only a 0.03 Å elongation of the Fe−Sδ distance). The trans-axial ligands are capable of rotating independently of each other in the reduced form, and this picture is only slightly perturbed in the oxidized one.

The introduction of the propionates and other heme side chains in model **2** produces significant effects. First, it is evident that the axial imidazole ligand has much less freedom to rotate. This is in agreement with the crystal structures of many cytochrome c systems, which show that the propionate groups are involved in hydrogen bonds and salt bridges with the nearby residues, such as Lys79.[23] Evidently, the protein matrix affects the orientation and mobility of His18 also through the arrangement of the propionate side chains of the heme. The present model **2** underlines the formation of strong hydrogen bonding involving one of the two propionate side chains and the Hδ1 atom of the Im ligand. In this case, even proton transfer may occur from the nitrogen to the oxygen atom. Moreover, following hydrogen bond formation, the dissociation of the methionine ligand readily occurs. Such a dissociation has been experimentally observed for the oxidized form only (e.g., upon addition of denaturant agents,[8] increase in temperature, variation of the pH,[15] etc.).

Finally, the calculation for model **3** with a hindering acetamide molecule shows that the strong hydrogen bonding is weakened to a form of electrostatic interaction. The latter still affects the freedom of the Im ligand, which can be related with the dissociation of Met80 from the heme. The calculations of all of the models also indicate that Met80 dissociation is easier for the oxidized form than for the reduced form **3R**.

These results well agree with many experimental findings; however, one must be aware of some possible shortcomings of the present computational approach. For instance, the loss of the octahedral geometry through the dissociation of one axial ligand could favor high-spin states for both the Fe(II) and the Fe(III) derivatives,[8,36] which have been neglected by this study. Also, the dissociative trend for the Fe−S bond could be caused by the limitations of DFT theory in describing the dispersive forces.

The very important result of this study is that, in the absence of the proprionate groups (model **1**), Fe−S bond dissociation is not observed. Likely, slight movements of the carboxylate

groups seem to switch on or off the electrostatic interactions between the propionate groups and the Im ligand; hence the strength of the iron−Im linkage is affected. In turn, this exerts a trans influence on the Fe−S bond and rules its eventual dissociation. In this context, also the oxidation state of the metal plays an important role.

**Acknowledgment.** We thank Dr. Paolo Giannozzi of Scuola Normale Superiore (Pisa, Italy) and Dr. Carlo Cavazzoni of CINECA (Bologna, Italy) for helpful discussions. Additional computer resources were provided by a grant of the CINECA Computer Center (Bologna, Italy) and by the European Center for Theoretical Studies (Trento, Italy). This work has been done with the financial support of FIRB 2001 project RBAU01HYZ8 of MIUR (Italy).

**Supporting Information Available:** Animations of **1R**, **1O**, **3R**, **3O**, and **4O** simulations. This material is available free of charge via the Internet at http://pubs.acs.org.

## References and Notes

(1) *Handbook on Metalloproteins*; Bertini, I., Sigel, A., Sigel, H., Eds.; Marcel Dekker: New York, 2001.
(2) *The Porphyrin Handbook*; Kadish, K. M., Smith, K. M., Guilard, R., Guiland, R., Eds.; Academic Press: Burlington, MA, 1999.
(3) *Cytochrome C: A Multidisciplinary Approach*; Scott, R. A., Mauk, A. G., Eds.; University Science Books: Sausalito, CA, 1996.
(4) *Bioinorganic Chemistry*; Bertini, I., Gray, H. B., Lippard, S. J., Valentine, J. S., Eds.; University Science Books: Mill Valley, CA, 1994.
(5) Marcus, R. A. *Rev. Mod. Phys.* **1993**, *65*, 599−610.
(6) Warshel, A.; Parson, W. W. *Q. Rev. Biophys.* **2001**, *34*, 563−679.
(7) Kitagawa, T.; Haruta, N.; Mizutani, Y. *Biopolymers* **2002**, *67*, 207−213.
(8) Bertini, I.; Turano, P.; Vasos, P. R.; Bondon, A.; Chevance, S.; Simonneaux, G. *J. Mol. Biol.* **2004**, *336*, 489−496.
(9) Simonson, T. *Rep. Prog. Phys.* **2003**, *66*, 737−787.
(10) Muegge, I.; Qui, P. X.; Wand, A. J.; Chu, Z. T.; Warshel, A. *J. Phys. Chem. B* **1997**, *101*, 825−836.
(11) Sharp, K. A. *Biophys. J.* **1998**, *73*, 1241−1250.
(12) Mao, J.; Hauser, K.; Gunner, M. R. *Biochemistry* **2003**, *42*, 9829−9840.
(13) Gray, H.; Winkler, J. R. *Proc. Natl. Acad. Sci. U.S.A.* **2005**, *102*, 3534−3539.
(14) Tan, M.; Balabin, I.; Onuchic, J. N. *Biophys. J.* **2004**, *86*, 1813−1819.
(15) Assfalg, M.; Bertini, I.; Dolfi, A.; Turano, P.; Mauk, A. G.; Rossell, F. I.; Gray, H. B. *J. Am. Chem. Soc.* **2003**, *125*, 2913−2922.
(16) Maity, H.; Maity, M.; Englander, S. W. *J. Mol. Biol.* **2004**, *343*, 223−233.
(17) Krishna, M. M. G.; Lin, Y.; Englander, S. W. *J. Mol. Biol.* **2004**, *343*, 1095−1109.
(18) Maity, H.; Maity, M; Krishna, M. M. G.; Mayne, L.; Englander, S. W. *Proc. Natl. Acad. Sci. U.S.A.* **2005**, *102*, 4741−4746.
(19) Pletneva, E. V.; Gray, H. B.; Winkler, J. R. *J. Mol. Biol.* **2005**, *345*, 855−867.
(20) Ott, M.; Robertson, J. D.; Zhivotovsky, V. G. B.; Orrenius, S. *Proc. Natl. Acad. Sci. U.S.A.* **2002**, *99*, 1259−1263.
(21) Baistrocchi, P.; Banci, L.; Bertini, I.; Turano, P.; Bren, K. L.; Gray, H. B. *Biochemistry* **1996**, *35*, 13788−13796.
(22) Banci, L.; Bertini, I.; Bren, K. L.; Gray, H. B.; Sompornpisut, P.; Turano, P. *Biochemistry* **1997**, *36*, 8992−9001.
(23) The PDB structures 1AKK, 1CCR, 1CHJ, 1CRC, 1CRG, 1CRI, 1CTY, 1FHB, 1GIW, 1HRC, 1LC1, 1N9C, 1OCD, 2FRC, 2YCC, 1YFC, 1YIC, 1CYC, 1J3S, and 1KX2 have been analyzed.
(24) (a) Bernstein, F. C.; Koetzle, T. F.; Williams, G. J.; Meyer, E. F. J.; Brice, M. D.; Rodgers, J. R.; Kennard, O.; Shimanouchi, T.; Tasumi, M. *J. Mol. Biol.* **1977**, *112*, 535−542. (b) RCSB Protein Data Bank. http://www.rcsb.org.
(25) Car, R.; Parrinello, M. *Phys. Rev. Lett.* **1985**, *55*, 2471−2474.
(26) Carloni, P.; Rothlisberger, U.; Parrinello, M. *Acc. Chem. Res.* **2002**, *35*, 455−465.
(27) Andreoni, W.; Marx, D.; Sprik, M. *ChemPhysChem* **2005**, *6*, 1671−1947.
(28) Giannozzi, P.; Angelis, F. D.; Car, R. *J. Chem. Phys.* **2004**, *120*, 5903−5915.
(29) Fantacci, S.; Angelis, F. D.; Sgamellotti, A.; Marrone, A.; Re, N. *J. Am. Chem. Soc.* **2005**, *127*, 14144−14145.
(30) Shaik, S.; Kumar, D.; de Visser, S. P.; Altun, A.; Thiel, W. *Chem. Rev.* **2005**, *105*, 2279−2328.
(31) Altun, A.; Guallar, V.; Friesner, R. A.; Shaik, S.; Thiel, W. *J. Am. Chem. Soc.* **2006**, *128*, 3924−3925.
(32) Rovira, C.; Carloni, P.; Parrinello, M. *J. Phys. Chem. B* **1999**, *103*, 7031−7035.
(33) Autenrieth, F.; Tajkhorshid, E.; Baudry, J.; Luthey-Schulten, Z. *J. Comput. Chem.* **2004**, *25*, 1613−1622.
(34) (a) te Velde, G.; Bickelhaupt, F. M.; van Gisbergen, S. J. A.; Fonseca Guerra, C.; Baerends, E. J.; Snijders, J. G.; Ziegler, T. *J. Comput. Chem.* **2001**, *22*, 931−967. (b) Scientific Computing & Modelling. http://www.scm.com.
(35) Perdew, J. P.; Chevary, J.; Vosko, S. H.; Jackson, K. A.; Pederson, M. R.; Singh, D. J.; Fiolhais, C. *Phys. Rev. B* **1992**, *46*, 6671−6687.
(36) Zucchi, M. R.; Nascimento, O. R.; Falconi-Alario, A.; Prieto, T.; Iseli, L. *Biochem. J.* **2003**, *370*, 671−678.
(37) Bartalesi, I.; Bertini, I.; Ghosh, K.; Rosato, A.; Turano, P. *J. Mol. Biol.* **2002**, *321*, 693−701.
(38) Baroni, S.; Corso, A. D.; de Gironcoli, S.; Giannozzi, P.; Cavazzoni, C.; Ballabio, G.; Scandolo, S.; Chiarotti, G.; Focher, P.; Pasquarello, A.; Laasonen, K.; Trave, A.; Car, R.; Marzari, N.; Kokalj, A. PWscf Home Page. http://www.pwscf.org.
(39) Vanderbilt, D. *Phys. Rev. B* **1990**, *41*, 7892−7895.
(40) Laasonen, K.; Pasquarello, A.; Car, R.; Lee, C.; Vanderbilt, D. *Phys. Rev. B* **1993**, *47*, 10142−10153.
(41) Perdew, J. P.; Burke, K.; Ernzerhof, M. *Phys. Rev. Lett.* **1996**, *77*, 3865−3868.
(42) Nosé, S. *Mol. Phys.* **1984**, *52*, 255−268.
(43) Frenkel, D.; Smit, B. *Understanding Molecular Simulation*; Academic Press: San Diego, 1996.
(44) Walker, F. A. *Chem. Rev.* **2004**, *104*, 589−615.
(45) Galstyan, A. S.; Zaric, S. D.; Knapp, E. W. *J. Biol. Inorg. Chem.* **2005**, *10*, 343−354.
(46) Moore, G. R. *FEBS Lett.* **1983**, *161*, 171−175.